Oceanologia (2019) 61, 412—426

Available online at www.sciencedirect.com

ScienceDirect

journal homepage: www.journals.elsevier.com/oceanologia/

ORIGINAL RESEARCH ARTICLE

Assessment of coastal vulnerability in Chabahar Bay due to climate change scenarios

Mahmoudreza Armanfar [a], **Hamid Goharnejad** [a,c,d,*], **Mahmoud Zakeri Niri** [b], **Will Perrie** [c]

[a] *Environmental Sciences Research Center, IslamShahr Branch, Islamic Azad University, IslamShahr, Iran*
[b] *Young Researchers and Elite Club, IslamShahr Branch, Islamic Azad University, IslamShahr, Iran*
[c] *Fisheries and Oceans Canada, Bedford Institute of Oceanography, Dartmouth, Nova Scotia, Canada*
[d] *Engineering Mathematics and Internetworking, Dalhousie University, Halifax, Nova Scotia, Canada*

Received 2 October 2018; accepted 7 March 2019
Available online 21 March 2019

KEYWORDS
Climate change;
Sea level rise;
Wave regime prediction;
Coastal vulnerability;
MIKE21 model

Summary A substantial body of research has shown that two key factors of global sea level rise are thermal expansion and melting of land-based ice, glaciers and ice sheets. Moreover, climate change may result in changes to wind speeds and directions, consequently resulting in contributions to variations in wind-wave components, wave heights and directions. In this research, climate change scenarios were used to assess the coastal vulnerability to the Chabahar port area due to global sea level rise, significant wave height changes and tidal regime effects. These three items were calculated separately using numerical models and the impacts of possible climate change scenarios were applied to estimate possible changes to these items by 2100. Significant wave heights for 25, 50 and 100-year return periods were evaluated. Based on statistical analysis, the maximum significant wave heights for the A2 and A1B scenarios were estimated at approximately 13.7 and 7.6, respectively. Since the main aim of this research was to assess the coastal zones at higher flood risk, therefore the mean global sea level rise, extreme values of significant wave heights and tidal heights were investigated. The height of sea during sea storms and for the most extreme case was calculated as 17.3 m and 11.2 m for A2 and the A1B scenarios, respectively. According to output maps of inundation areas, large coastal zones in the Chabahar port area are at risk due to the sea storms and possible climate change.

* Corresponding author at: Department of Civil Engineering, Environmental Sciences Research Center, IslamShahr Branch, Islamic Azad University, IslamShahr, Iran. Tel.: +98 9127144265.
E-mail address: Hgn1982@gmail.com (H. Goharnejad).
Peer review under the responsibility of Institute of Oceanology of the Polish Academy of Sciences.

https://doi.org/10.1016/j.oceano.2019.03.001

1. Introduction

During the past two decades, scientists and politicians from developed and developing countries have become increasingly interested in global warming and climate change. Although climate change, as a natural phenomenon, occurs on a variety of scales, some as long as a thousand years or more, changes due to human activities have resulted in increasing volumes of greenhouse gases in the atmosphere. The recent climate changes have perhaps been more intense than the earlier ones, happening some two million years ago (IPCC, 2001; Stone et al., 2003). According to the IPCC report, a global warming of 0.89°C has occurred in the global ocean temperature over the period 1901—2012, whereas this figure was 0.74°C within 1951—2003 (IPCC, 2007). Recent studies have shown that in the 20th century the mean sea level and average wind speed increased by as much as 30 cm and 1 m/s, respectively (WCRP, 2018). Related changes, such as stronger hurricanes suggest that coastal areas are becoming more vulnerable. Furthermore, due to specific topography, population density, as well as economic parameters, coastal zones are recognized as sensitive climate areas in the world (Tragaki et al., 2018). For example, in the United States, approximately 25 million people live in areas vulnerable to coastal flooding.

Climate change can affect coastal areas in a variety of ways. The effects of climate change include a rise of mean sea level, significant wave height changes due to wind speed and direction changes, and the severity of oceanic storms. These factors can seriously endanger coastal structures, tourism, fisheries, transportation systems, and even offshore energy farms. As a result, it is necessary to carry out studies to analyze the impact of climate change on coastal zones. In previous studies, global mean sea level rise due to the increased water temperature, ocean internal expansions, as well as melting glaciers have captured the interest of several investigations (Bindoff et al., 2007; Houghton et al., 2001; Pfeffer et al., 2008).

On the other hand, research conducted over the past decade has suggested that wind characteristics including speed and direction are influenced by climate changes, and hence can result in changes in wind-wave heights. Over a 100-year period to 2100, Chini et al. (2010) projected that wind-wave heights may increase up to 12 percent because of the climate change impacts on wind speed over the eastern coast of England. Kamranzad et al. (2013) used three emission scenarios, A1B, A2 and B1, to investigate the impact of climate change on wind speed and direction in the area around Chabahar. Vanem et al. (2012) considered the impact of climate change on the wave climate of the global ocean. They investigated 12 specific zones including the North, South, and middle Atlantic, North East, North West, and South Pacific, Gulf of Mexico, Indian Ocean, Tasmanian Sea, Mediterranean Sea, and West Australia ocean areas, and found a correlation between CO_2 changes and significant wave heights under A2 and B1 emission scenarios. At 90% confidence level, the results showed that the maximum and minimum changes in the significant wave heights occurred in the A2 and B1 climate change scenarios, respectively.

Dastgheib et al. (2016) analyzed the effect of climate change in waters off the Vietnamese coastline. Two periods of 1981—2000 and 2081—2100 were considered to represent the present and the future climate periods, respectively. They found that for northern Vietnam coastal areas, the mean significant wave heights decreased by some 8 cm compared to the present climate, and the wave periods increased by 0.2 s; whereas, for central and southern coastal areas, the mean significant wave heights and wave periods showed 5—7 cm and 0.08 and 0.16 s increases, respectively. In the meanwhile, Duan et al. (2014) studied the effects of climate change on wave characteristics in 10 zones around the Japanese coasts using observed buoy data from 1988—2012. They used sea surface temperature (SST), Multivariate ENSO Index (MEI), Southern Oscillation Index (SOI), Arctic Oscillation Index (AOI), Pacific Decade Oscillation Index (PDOI), and North Pacific Index (NPI) to calculate correlations between the meteorological indexes and the wave parameters, significant wave height, and wave period. They finally concluded that mean significant wave heights and wave periods at all zones increased 49.65 cm and 0.25 s, respectively.

In the North Atlantic during the fall hurricane season, Guo et al. (2015) studied the impacts of climate changes on surface waves. They used WAVEWATCHIII wave model and winds from the Canadian global climate model, CGCM3.1, dynamically downscaled using a regional climate model, and A1B and B1 climate change scenarios to elucidate the changes that might occur during 2040—2069 in wave regimes. They suggest that compared to the present climate represented as 1970—1999 in their study, wave heights may increase in the northeast North Atlantic, whereas in other areas such as mid-latitudes, decreases are expected, with associated changes in winds. Mitchell et al. (2015) simulated waves using WAVEWATCHIII under the A1B scenario to study the effect of climate change on potential wave energy off the coasts of England. They found a small reduction in mean significant wave heights during 2040—2069; however, the reduction was so trivial that no reductions are expected in potential wave power levels. Wave power is directly related to the squared significant wave height and the period.

Wandres and Pattiaratchi (2017) studied the possible changes of the wave climate off the southwestern Australian coast under two atmospheric greenhouse gas concentration pathways using SWAN wave model for RCP4.5 and RCP8.5 climate change scenarios. They used wind data over the period of 1986—2005 to model wave characteristics and then they used the calibrated model to simulate the wave regime during 2081—2100. Results suggest a 2—4% increase in mean significant wave heights in nearshore areas and a small change in the dominant wave directions. Moreover, in winter months, the longshore wave energy flux, which is responsible for littoral drift, is expected to increase by up to 39% and 62% under the RCP4.5 and RCP8.5 greenhouse gas concentration pathway with SLR, respectively. Karymbalis et al. (2012) assessed the vulnerability of the southern coast of the Gulf of Corinth due to the sea level rise. They concurred that 57.0 km of coastline (corresponding to 38.7% of the whole coastline), is highly vulnerable because of low topography.

Likewise, Pantusa et al. (2018) investigated vulnerable areas of Apulian coastline of southern Italy using the coastal vulnerability index (CVI), which is described as follows. They used 10 parameters (relative sea-level change, mean significant wave height and mean tide range, etc.) to assess CVI in the study area. Their results confirmed the importance of CVI

to assess coastal vulnerability with respect to climate change. Pendleton et al. (2005) also studied the vulnerability of Cape Hatteras using this approach. CVI ranks the following in terms of their physical contribution to sea-level rise-related coastal change: geomorphology, regional coastal slope, rate of relative sea-level rise, historical shoreline change rates, mean tidal range, and mean significant wave height.

Regarding mean sea level rise, many studies have been carried out worldwide and on local scales (Horton et al., 2008; Jevrejeva et al., 2010; Pfeffer et al., 2008; Rahmstorf, 2007). Mean sea level rise in the study area has been discussed by Goharnejad et al. (2013). They used A1B and A2 scenarios to study sea level changes to 2100 and reported that the maximum expected sea level rise is 60 cm. The current study continues the previous work by Goharnejad et al. (2013).

In this study, we modeled tidal flows and wind-waves regimes in the Chabahar port area. Since tidal currents are not directly affected by climate change, hence wind-waves have been calculated due to climate change under two scenarios, namely A1B and A2, to 2100. The A2 and A1B scenarios represent the possibly extreme and mean climate changes, respectively. Thus, significant wave height extreme values are estimated for return periods of 25, 50 and 100 years using three probability distribution functions. The mean global sea level rise has been extracted from the previous study by Goharnejad et al. (2013). Finally, in order to assess the vulnerability of the Chabahar coastal zone, the three above-mentioned parameters have been summarized.

2. Study area

Chabahar with a total area of 17,155 km^2 is located on the southeastern part of Iran along the Oman Sea and close to the Indian Ocean. As seen in Fig. 1, Chabahar port area is more than 11 km^2 with the altitude of 7 m above sea level and is located between 60°20′ to 60°32′E longitudes, and 25°17′ to 25°27′N latitudes. Chabahar Bay with the geometry of Ω shape and without any considerable rivers has moderate tropical weather. The summer monsoon winds from the Indian subcontinent make Chabahar the coolest southern port in the summer and the warmest port of Iran in the winter. It has an average maximum temperature of 34°C and an average minimum temperature of 21.5°C.

3. Methodology and data collection

3.1. Spectral wave model setting and data used

In order to study the wave regimes in coastal areas off Chabahar, it is necessary to have geographic data (boundaries and bathymetry data), wind data (speed and direction), Buoy wave data, and sea level pressure data. In this study, the Spectral Wave analysis (SW) and Flow Model (FM) modules of MIKE21 were used with the aim of hindcasting offshore wave characteristics using available wind data. Waves were numerically modeled in the study area using the SW model, which is a dynamic modeling system based on the spectral wave model and implemented on an irregular unstructured grid often used in coastal areas, estuaries, and rivers. Danish Hydraulic Institute initially prepared this wave model in the version 2005 of DHI software (DHI, 2005). The model can solve the energy transfer equation with wave source and sink terms to predict the developing wave field.

The governing equation of MIKE21 wave model is the spectral action balance equation, which for Cartesian coordinates is:

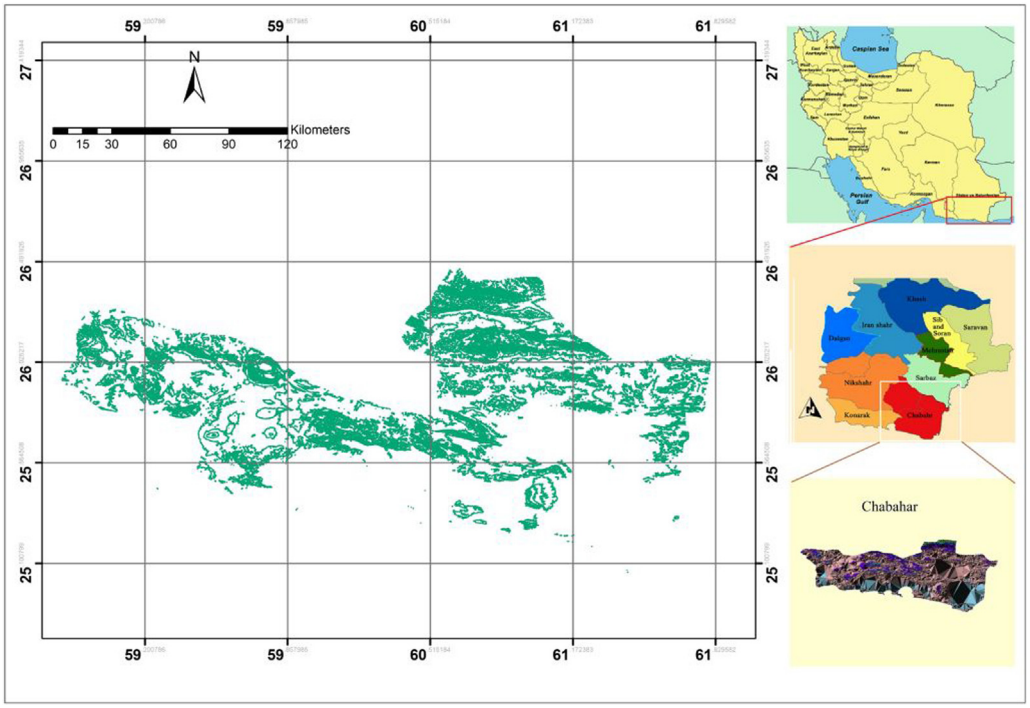

Figure 1 General view of the study area.

$$\frac{\partial}{\partial t}N+\frac{\partial}{\partial x}C_{g,x}N+\frac{\partial}{\partial y}C_{g,y}N+\frac{\partial}{\partial \sigma}C_{g,\sigma}N+\frac{\partial}{\partial \theta}C_{g,\theta}N=\frac{S}{\sigma}, \quad (1)$$

where σ is the relative frequency, θ is wave direction, N is wave action density, which is equal to the energy density divided by the relative frequency ($N(\sigma, \theta) = E(\sigma, \theta)/\sigma$) and C_g is the propagation velocity of wave action in (x, y, σ, θ) space. The last term on the left side of the equation denotes the effects of refraction and shoaling. The source term on the right of the wave transfer equation is defined as follows:

$$S = S_{in} + S_{nl} + S_{dis} + S_{ot} + S_{surf}, \quad (2)$$

where S_{in} represents energy transfer from wind to the waves, S_{nl} represents energy transfer from one frequency to another by nonlinear wave-wave interactions, S_{dis} is wave energy dissipation under the effect of the white-capping, S_{ot} is the wave dissipation due to bottom friction, and S_{surf} represents wave dissipation resulting from the wave breaking in a shallow area.

Bathymetry data at 1-min resolution (about 1.7 km) were collected from National Centers for Environmental Information, NOAA (https://www.ngdc.noaa.gov/mgg/bathymetry/relief.html).

Because there were no comprehensive observed data of the wind and waves in the study area at the beginning of the study, a large scale model that covered the Oman Sea and a small part of Indian Ocean with the eastern longitudes extending from 56° to 66° and the northern latitudes extending from 21° to 27°, was deployed (see Fig. 2). Moreover, wind data were extracted from ERA-Interim reanalysis data (Jan. 1979–present) with 0.25° spatial and 6-h temporal resolutions at 10 m reference height above sea level as wave model inputs (https://www.ecmwf.int/en/forecasts). In the numerical wave model, wind data were used for two periods within 1971–2000 and 2006–2016, as calibration and verification periods, respectively.

Fig. 3 shows the average wind rose along the Chabahar coastline based on ECMWF data.

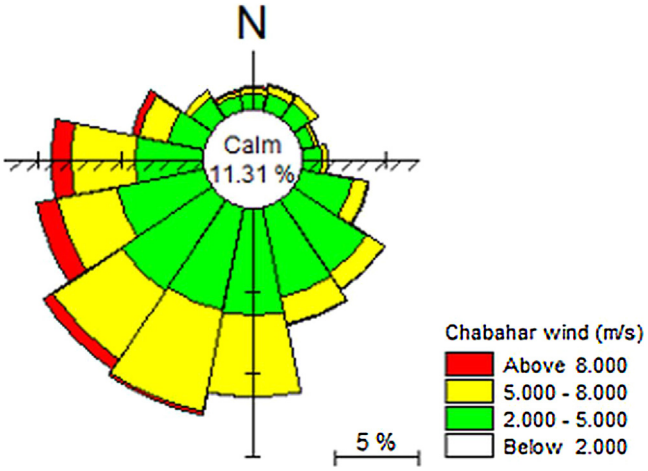

Figure 3 Chabahar local wind rose based on ECMWF data (2006–2016).

As seen, the dominant winds blow from south and southwest. Table 1 also represents the monthly minimum and maximum wind speed, as well as the dominant direction of the Chabahar local winds.

Determining the time step is one of the most important parts of a wave model set up. Large time steps, on one hand, require fewer integration steps and higher execution of model computation. However, excessively large time steps may decrease model accuracy. In this regard, with suitable numerical experimentation, the appropriate time steps were obtained in both large and local scales for the current and wave models of MIKE21 (see Table 2).

Moreover, five other parameters are needed to calibrate the model. The default and calibrated values are shown in Table 3. As seen in this table, the bottom friction is a sensitive factor in the wave model, whereas other parameters showed no significant effects on the results.

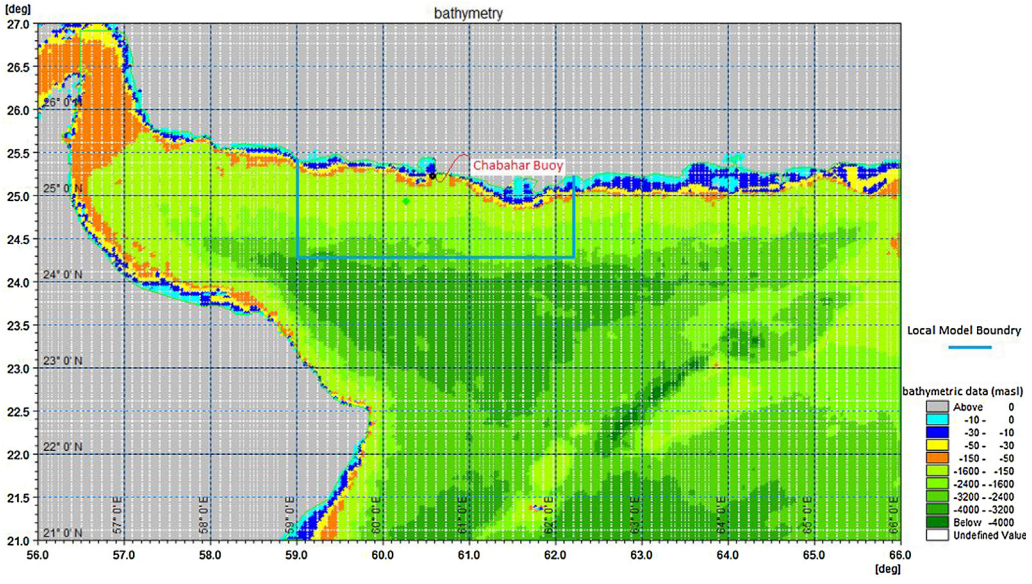

Figure 2 Large scale model bathymetry, Chabahar buoy, and local model boundary in the Oman Sea and the Indian Ocean.

Table 1 Wind characteristics in the study area based on ECMWF wind data (2006–2016).

Month	Wind speed (m/s)		Dominant wind direction
	Minimum	Maximum	
January	0.08	10.71	WSW-SW
February	0.10	11.98	SW- WSW
March	0.09	11.50	WSW-SW
April	0.02	12.37	WSW-SW
May	0.21	11.51	SW-SSW
June	0.21	18.4	S-SSW
July	0.36	10.65	S-SSE
August	0.40	10.37	S-SSE
September	0.16	8.6	S-SE-SW
October	0.11	7.57	SSW-WSW
November	0.16	8.81	SW-SSW
December	0.04	11.45	N-W

Table 2 Time steps for large and local scales for ocean current and wave models.

Scale	Current model time step (s)			Wave model time step (s)		
	Appropriate	Maximum	Minimum	Appropriate	Maximum	Minimum
Large	60	600	60	600	3600	300
Local	30	300	30	60	600	30

Table 3 Appropriate values for parameters in the wave model.

Parameter	White capping (C_{dis})	White capping (δ)	Wave breaking (γ)	Wave breaking (α)	Bottom friction
Default	4.5	0.5	0.8	1	0.04
Calibrated	4	0.5	0.8	1	0.13

Once the effective parameter values were determined, the model was used to simulate a one-month period and the results were compared with buoy data. The buoy wave data were obtained from the Chabahar Buoy station. It was established in 1996 and the completeness percentage is 97% (see https://www.psmsl.org/data/obtaining/stations/1881.php). These data were used to calibrate and validate the wave model results (see http://marinedata.pmo.ir). Buoy characteristics are presented in Table 4. Thereafter, the wind-wave model was verified for an additional three one-month periods. The calibration and verification results for these periods are shown in Table 5.

3.1.1. Spectral wave model performance

In order to evaluate the model performance, statistical parameters between observed and modeled data were calculated as follows:

bias $\quad \text{Bias} = (S-O),$

root mean squared errors $\quad \text{RMSE} = \sqrt{\frac{1}{N}\sum(S_i-O_i)^2},$

correlation coefficient $\quad \text{CC} = \frac{\sum(S_i-S)(O_i-O)}{\sqrt{\sum(S_i-S)^2\sum(O_i-O)^2}},$

Table 4 Chabahar buoy properties.

Station	Type	Coordinate		Depth (m)	Available parameters
		Latitude	Longitude		
Chabahar	Datawell	25.283	60.616	17	• Mean wave direction • Wave period • Significant wave height

Table 5 Calibration and verification periods for the wave model.

Calibration period	Verification period 1	Verification period 2	Verification period 3
July 2016 31 days	October 2015 31 days	January 2012 31 days	April 2011 30 days

Table 6 Results of model performance indices for the Chabahar buoy (2006–2016).

Parameter	Normal range	Ideal range	Calibration	Validation 1	Validation 2	Validation 3
Bias (m)	0.2–0.5	<0.3	0.150	0.008	0.015	0.003
CC	0.75–0.90	>0.8	0.830	0.930	0.870	0.910
RMSE (m)	0.1–0.7	<0.5	0.189	0.048	0.118	0.140
SI	0.15–0.35	<0.3	0.291	0.095	0.181	0.080

dispersion coefficient $\mathrm{SI} = \frac{\sqrt{\frac{1}{N}\sum(S_i - O_i)^2}}{O}$,

where O_i is the observed value at the ith time step, S_i is a forecast value at the same moment of time, N is the number of time steps and O and S are the mean values of the observed data and forecast results, respectively. Table 6 depicts the results of the model performance indices. Columns 2 and 3 show the normal and ideal ranges of each index, implying that the wave model is sufficiently accurate to estimate wave climate features. Meanwhile, Fig. 4 illustrates the modeled and observed significant wave heights.

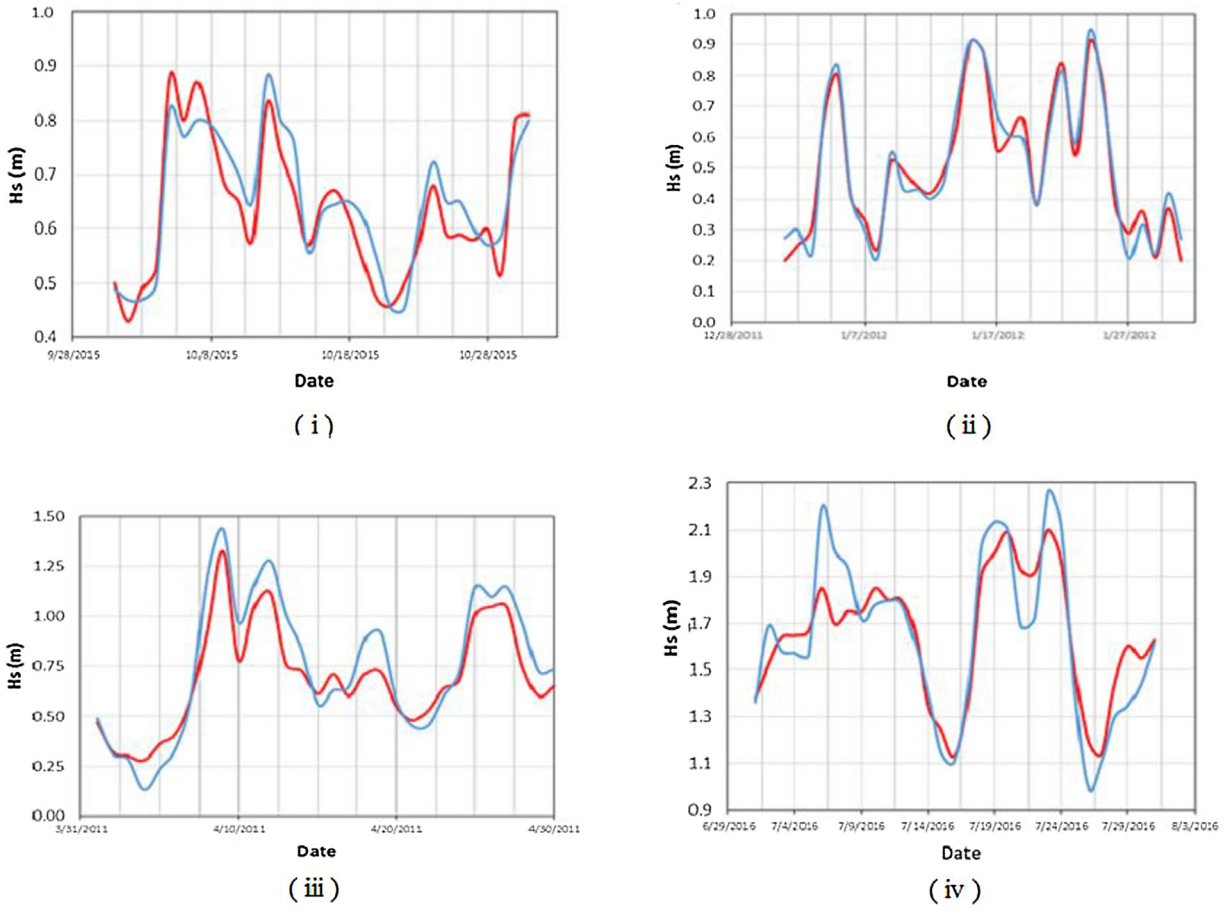

Figure 4 Time series of the modeled and observed significant wave heights at Chabahar station. (i) Calibration period (July 2016); (ii) Verification period 1 (October 2015); (iii) Verification period 2 (January 2012); (iv) Verification period 3 (April 2011); red line: observed significant wave height; blue line: modeled significant wave height. (For interpretation of the references to color in this figure legend, the reader is referred to the web version of this article.)

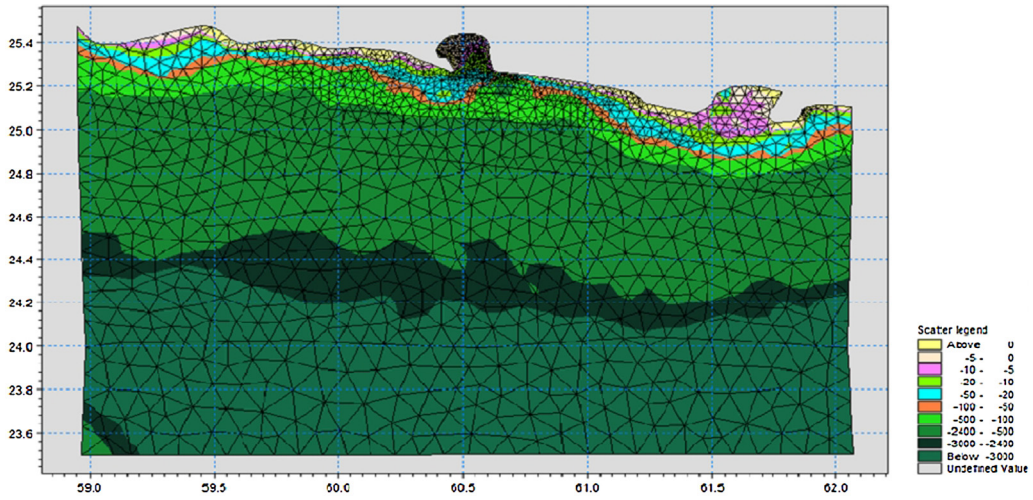

Figure 5 The local model with triangular meshes in the study area.

In the next step, boundary conditions including time series of wave parameters were extracted from the large area model and were used as boundary conditions for the local model. The local model with triangular meshes is shown in Fig. 5. The optimization of the number of nodes and elements is an important part of wave modeling. Thence, numerical experimentation with several model-runs with different meshes were executed and eventually, the number of elements and nodes were determined as 2484 and 1453, respectively. As shown in Fig. 5, the mesh sizes in deeper water areas are bigger than those of shallow water areas, which are closer to the coastline.

3.1.2. Spectral wave model outputs

Once the accuracy of the wind-wave model performance was confirmed by statistical parameters, the model was run for 11 years, from 2006 to 2016. Significant wave height, wave period, wave direction and the frequency of occurrence (%) for these parameters are shown in Figs. 6 and 7.

3.2. Flow model setting and data used

In order to calculate the sea surface tidal currents and to consider the tidal effects on coastal areas, the current model was run over the local model domain. The wave breaking and tidal currents are among the most important parameters needed to determine the dominant wave regime in the study area (Rahimipouri et al., 2006). Thus, to set up a flow model, radiation stress data (S_{xx}, S_{xy}, and S_{yy}), local tidal parameters, as well as wind data are required. A further point of interest is that the number of elements and nodes were the same as those used for the spectral wave model, and the radiation stress data were taken from the spectral wave model and used as input parameters in the flow model. Model calibration was conducted during 3.15.2012 to 5.15.2012, and the verification period was from 11.19.2014 to 3.19.2015. The calibration and verification periods are different from those of the SW wave model because we used a different source of observed tidal data, and our recorded data

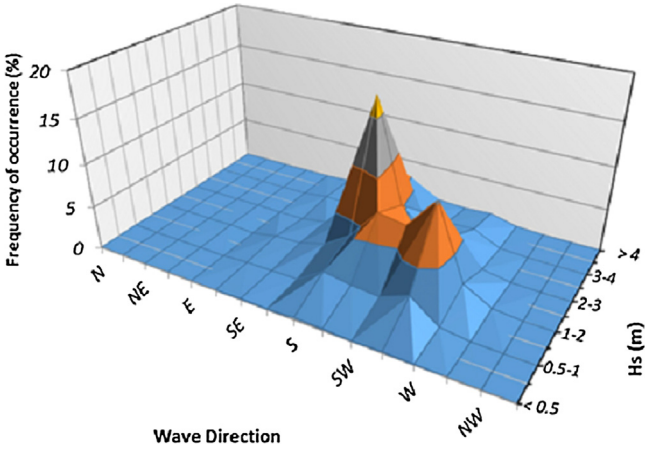

Figure 6 Frequency of occurrence (%) for significant wave height and wave direction at the Chabahar buoy location (2006—2016).

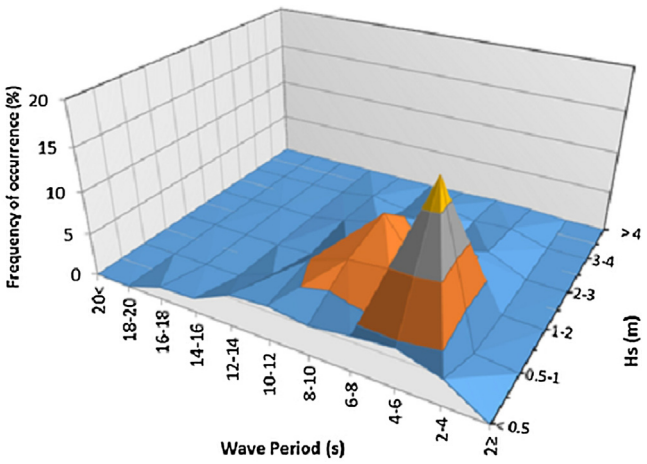

Figure 7 Frequency of occurrence (%) for significant wave height and wave period at the Chabahar buoy (2006—2016).

Table 7 The harmonic parameter values at Chabahar (Shirinmanesh and Chegini, 2014).

M2		S2		K1		O1	
Phase	Amplitude	Phase	Amplitude	Phase	Amplitude	Phase	Amplitude
267.3	0.62	299.6	0.24	34.5	0.4	35.8	0.2

have better quality during these selected periods. The main harmonic tidal parameters at Chabahar are extracted as recorded in Table 7 (http://www.tidetablechart.com/tides/hightide_lowtide/64110/Chabahar and http://marinedata.pmo.ir/).

Time series of tidal data were extracted from the flow model as shown in Fig. 8. In order to assess the flow model performance, the mentioned statistical indices were calculated and the results are presented in Fig. 9 and Table 8. Our results suggest that the flow model performance is acceptable and the output parameter series can be used with high reliability. Using the flow model outputs, the minimum and maximum sea level due to tidal flows are shown in Table 9. The results indicate that the minimum and maximum water levels during these 11 years are 1.69 and 2.96 m, respectively.

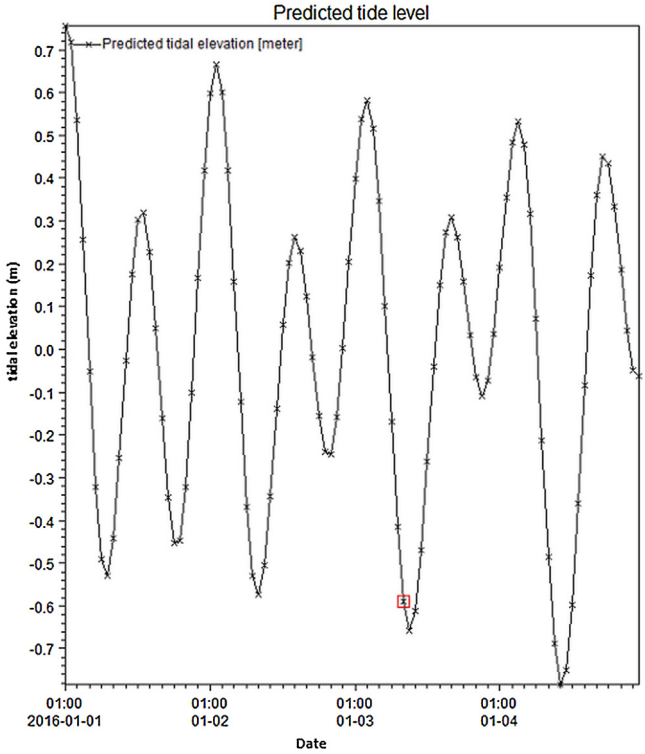

Figure 8 Predicted tidal level at Chabahar.

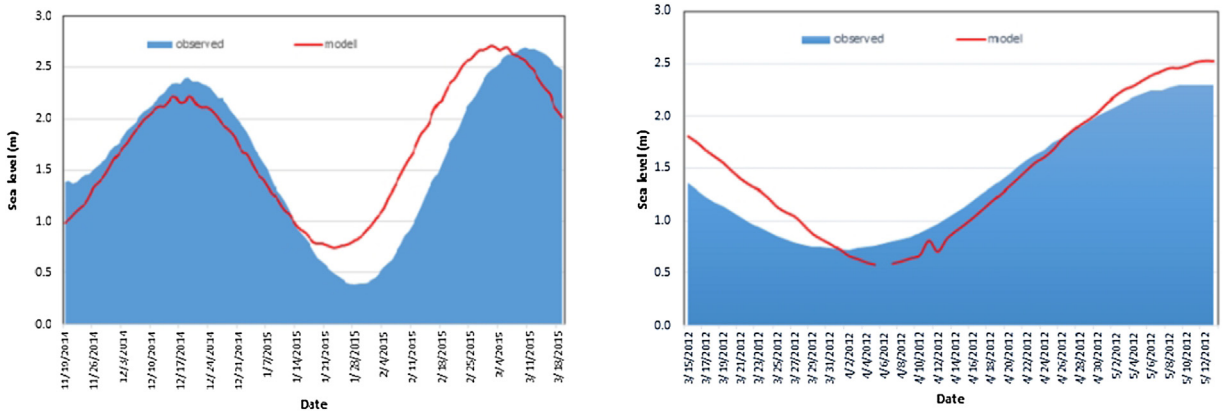

Figure 9 Time series of modeled and observed sea level due to tidal flows during two different periods.

Table 8 Error parameters between observed and modeled data during calibration and verification time periods.

Parameter	Bias (m)	CC	RMSE (m)	SI
Calibration	0.09	0.81	0.16	0.20
Verification	0.17	0.80	0.23	0.28

Table 9 Minimum and maximum sea level (2006–2016).

Year	Minimum sea level (m)	Maximum sea level (m)
2006	1.69	2.96
2007	1.76	2.70
2008	1.77	2.68
2009	1.76	2.93
2010	1.80	2.70
2011	1.72	2.85
2012	1.77	2.84
2013	1.80	2.70
2014	1.79	2.79
2015	1.86	2.61
2016	1.85	2.79

3.3. Impact of climate change

There are several global climate models that attempt to estimate the effects of climate change. In this research study, the Coupled Global Climate Model (CGCM3) was used and two emission scenarios, A2 and A1B, were selected (see http://climate-scenarios.canada.ca). Because of the large spatial and temporal scales of these data, downscaling is needed to describe climate model outputs. Downscaling is the process by which coarse-resolution GCM outputs are translated into finer resolution climate information, so that they can better account for regional climatic influences, such as local topography. The resolution of CGCM3.1 data is inappropriate for fine-resolution modeling of wave regimes. On the other hand, output time steps in GCM models are often monthly whereas modeling of local wave parameters needs hourly data. Hence, downscaling is an essential procedure for preparing input data. Generally, three main downscaling methods are available, including dynamical, statistical and combination of dynamical and statistical methods (Gutmann et al., 2012).

In this study, a Change Factor Methodology (CFM) has been applied, which is a combined method of dynamical and statistical approaches for spatial downscaling of GCM data (Trzaska and Schnarr, 2014). This method is consistent with the methods used by Kamranzad (2014) in the Persian Gulf to estimate wave power, and Breslow and Sailor (2002), in the U.S. for approximating wind power. In order to confirm the reliability of climate models outputs, it was necessary to initially compare observed and climate data. In this regard, a period was determined as a control period and the collocated data were examined. Comparing the ECMWF and CGCM3.1 wind data revealed that CGCM3.1 wind data were often underestimated. Hence, equations 3 and 4 were used to re-calibrate the CGCM3.1 wind data. The modification of CGCM3.1 wind data for monthly averages of absolute wind components is calculated by:

$$\beta_u = \frac{|u|_{\text{ECMWF(monthly average)}}}{|u|_{\text{CGCM3.1(monthly average)}}}, \tag{3}$$

$$\beta_v = \frac{|v|_{\text{ECMWF(monthly average)}}}{|v|_{\text{CGCM3.1(monthly average)}}}, \tag{4}$$

in which, β_u and β_v represent the modification factors for u and v components of the wind speed, respectively.

Figs. 10–13 depict ECMWF data ratio to A1B and A2 data in the 4 periods (July, January, October, and April) of calibration and verification.

Wind speed data taken from GCM climate change scenarios and ECMWF were compared with each other and results are depicted in Fig. 14. It is clear that the wind speed ratios between ECMWF data and A2 scenario are higher than those of the A1B scenario, which implies that A1B data and ECMWF data are more similar.

Once CGCM3.1 wind data were downscaled for A1B and A2 scenarios, the spectral wave model was run with modified

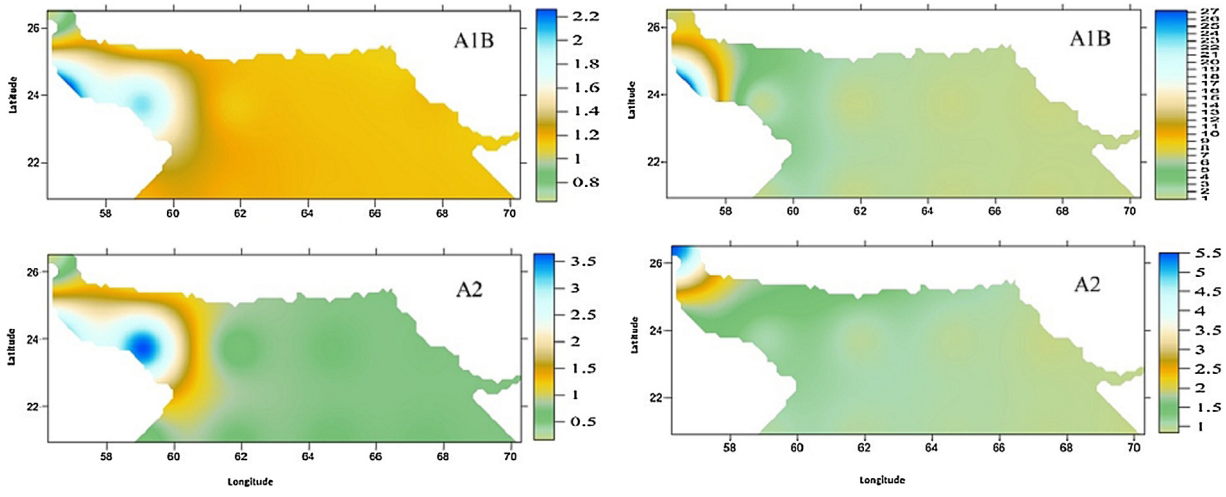

Figure 10 β_u (left) and β_v (right) for A1B and A2 scenarios in July (1981–2010).

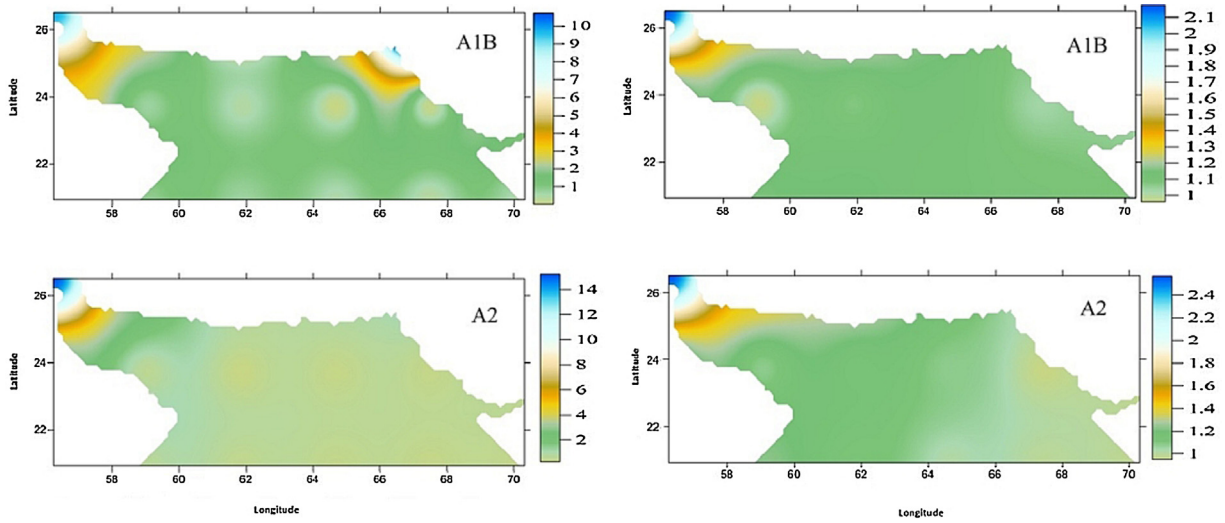

Figure 11 β_u (left) and β_v (right) for A1B and A2 scenarios in January (1981–2010).

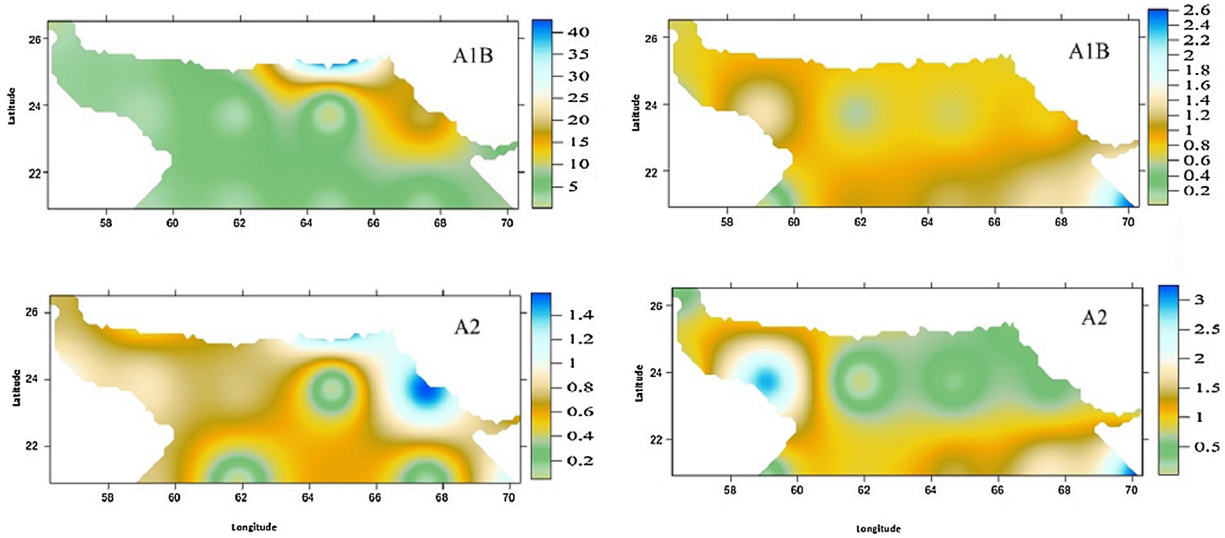

Figure 12 β_u (left) and β_v (right) for A1B and A2 scenarios in October (1981–2010).

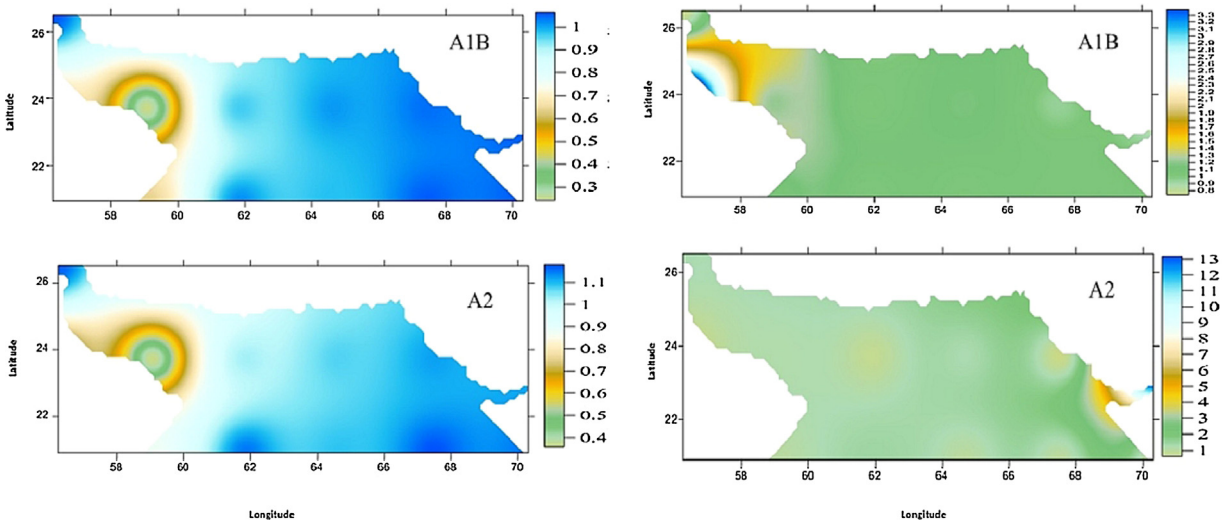

Figure 13 β_u (left) and β_v (right) for A1B and A2 scenarios in April (1981–2010).

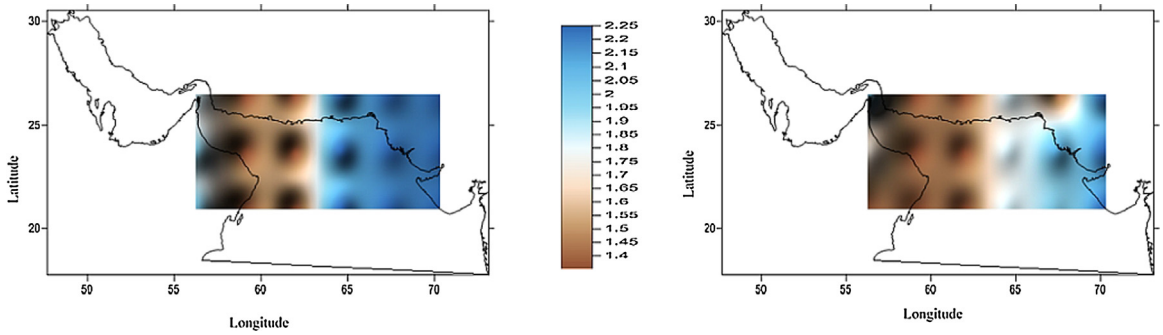

Figure 14 Comparison of wind speed ratios for (i) A2 climate change scenario and (ii) A1B climate change scenario to the ECMWF wind speed data for the present climate (1981—2010).

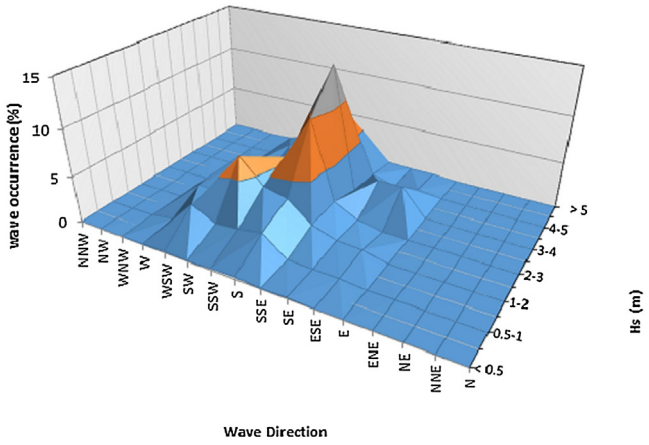

Figure 15 Frequency of occurrence (%) for significant wave height (Hs) and wave direction at Chabahar for A1B scenario (2071—2100).

climate change wind data for 30 years, 2071—2100. Wind model implementation results using A1B and A2 scenarios for climate data of years 2071—2100 are provided in Figs. 15—18, respectively.

Furthermore, as we should consider the global mean sea levels in our study, we used the results from Goharnejad et al. (2013). Their study showed that sea levels in southern seas of Iran are increasing because of thermal expansion and melting glaciers. According to their results for Chabahar, the mean sea level rise by 2100 for A1B and A2 are estimated to be 48 and 60 cm, respectively.

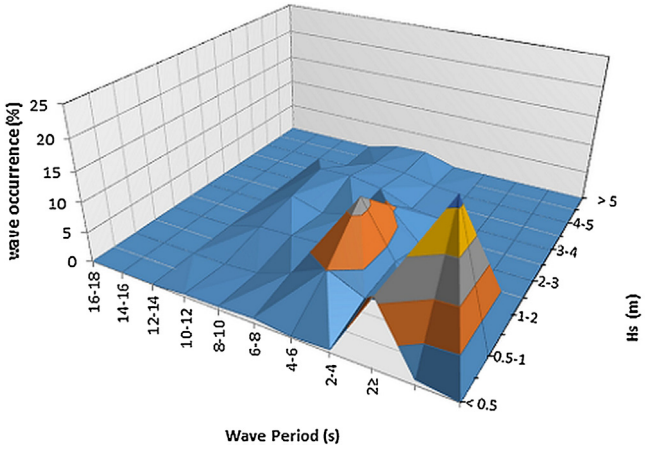

Figure 16 Frequency of occurrence (%) for significant wave height (Hs) and wave period at Chabahar for A1B scenario (2071—2100).

4. Discussion and results

We have calculated the wave characteristics for an 11-year period (2006—2016) representing the present time and a 30-year period (2071—2100) representing the future; the results are shown in Figs. 6 and 7. Accordingly, over 65% of the mean significant wave heights are smaller than 1 m, the majority of the waves have a period of less than 8 s, and travel from the south. The waves in the Oman Sea are influenced by several phenomena including monsoon fronts, local winds, and tropical typhoons. Since Chabahar is an oceanic port, it is influenced by swells coming from the Indian Ocean and the Arabian Sea; thus wind roses in this area are different from other parts of the Oman Sea. Moreover, due to the Arabian Peninsula, warm regional winds blow, in some months, from the southwest causing southwesterly waves to emerge. In general, mean significant wave heights of more than one meter often occur in June to September during summer monsoon phenomena. The maximum wave height for the 11-year period is 7 m with about 10 s wave period and direction toward the south, which are seen essentially every year in July. The mean wave height is 0.8 m and the mean wave period is calculated as 3.5 s. With respect to 11-year occurrences, the mean significant wave height is 2.5 m with a period of 5.7 s. Wave heights between 0.5—1.0 m have the maximum frequency of occurrence.

The ocean current flow direction is often from east to west turning towards the north at about Chabahar Bay. Sea level for the east-west current flow is between 1.7—2.8 m (Fig. 19i). Sometimes, additional weak flows travel from south-west and west directions into the study area, especially in the winter. In such cases, the maximum change in water level is less than 1.5 m (Fig. 19ii).

4.1. The effects of climate change

Studies have revealed that climate change influences the wave climate (Wojtysiak et al., 2018). The results of wave modeling for years 2006—2016 indicate that about 65% of the

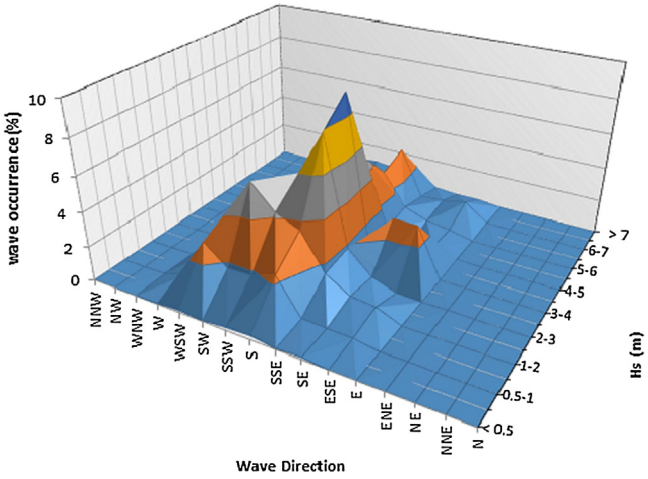

Figure 17 Wave occurrence (%) based on significant wave height (Hs) and wave direction in Chabahar for A2 scenario (2071—2100).

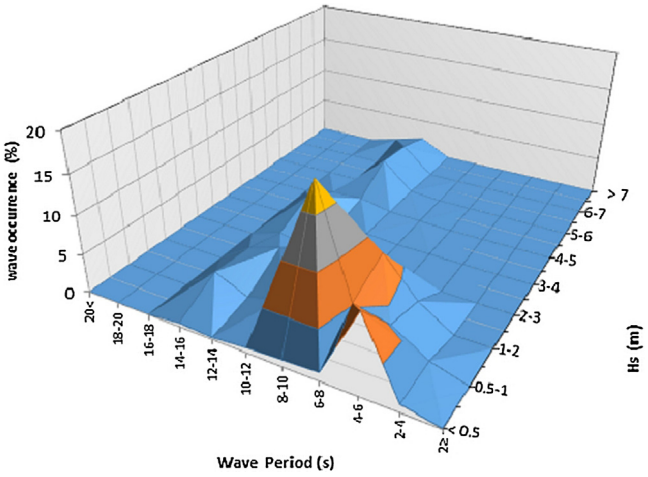

Figure 18 Wave occurrence (%) based on significant wave height (Hs) and wave period in Chabahar for A2 scenario (2071—2100).

wave heights are less than 1 m, of which 48% and 17% of these waves have wave periods less than, and more than, 10 s, respectively. In both climate change scenarios, approximately 50 percent of mean significant wave heights are 1 m or less. According to the wind-wave model results for A1B and A2 scenarios, it is suggested that although there is no considerable difference between wind speeds under A1B and A2 scenarios in Chabahar bay, wind speeds for A2 scenario in other areas of the integration, especially along the eastern boundary longitudes towards the Indian Ocean are much more than corresponding wind speeds under A1B scenario. In current climate conditions, most mean significant wave heights more than 1 m are observed during monsoon conditions between 1—2 m, and during hurricane conditions, wave heights with more than 4 m height have been observed in numerical results. According to these results, mean significant wave heights of 1 m or more during 2071—2100 would be expected in approximately 50% of the total distribution of waves where wave frequency is 2—4. Therefore, according to the A2 scenario, it is projected that longer waves will be developed during this climate scenario. On the other hand, more swells are expected to travel into Chabahar harbor in the future.

4.2. Wave characteristics in current conditions and climate change scenarios

As depicted in Fig. 6, in current conditions, more than 50% of the recorded waves travel from south and southwest directions relative to Chabahar Bay. Moreover, 4.19% of the mean significant wave heights are more than 4 m, 13.51% are between 3—4 m, 32.14% between 2—3 m, 39.38% between 1—2 m, 9.94% between 0.5—1 m, and only 0.83% are less than 0.5 m. According to Fig. 7, most wave periods were seen in the range 4—6 s with the mean significant wave heights 0.5—1 m, whereas wave periods with 8—10 s periods have 23.54% frequency of occurrence. In addition, the wave periods with over 14 s have a relatively rare frequency of occurrence.

Regarding A1B scenario, the majority of waves travel from the south with a frequency of occurrence of 38.3% followed by those from the south-southwest with a frequency of occurrence of 17.6%. Under this scenario, more than 70% of the waves travel from south and southwest. Around 25% of the mean significant wave heights of 2—3 m also come from the south. Furthermore, 24.1% and 21.5% of waves have

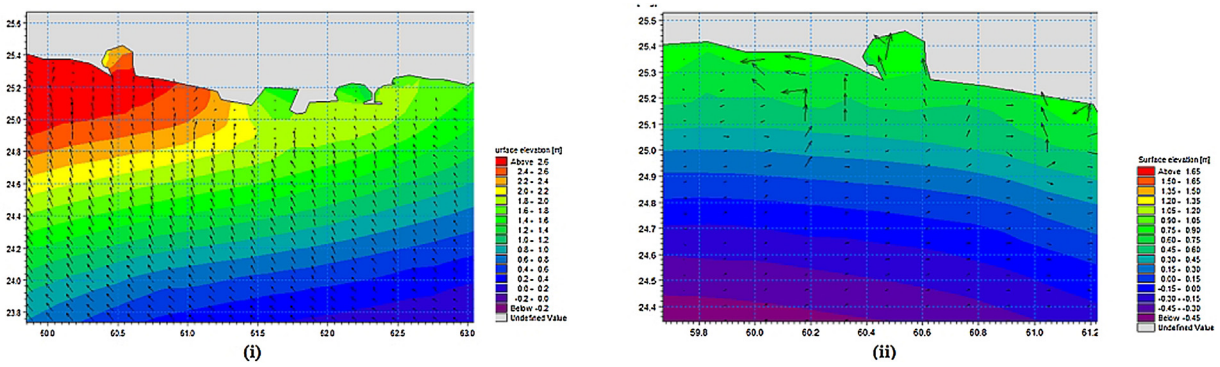

Figure 19 The current flow direction in Chabahar Bay: (i) the dominant flows in the study area and (ii) weak winter current flows.

periods of 8—10 and 2—4 s, respectively, which show that wave periods will decrease in the A1B scenario in comparison with present climate conditions. In addition, approximately 21.59% of the waves with periods of 2—4 s have the height of 0.5—1 m.

Concerning A2 scenario, 35.31% of the waves travel from the south, 18.3% from the south-southwest, 14.1% from the southwest, and 11.5% of the waves come from the west-southwest. This implies that around 80% of the waves move from south and west to the coast with mean significant wave heights of 2—4 m. Moreover, in 25.6% of the waves, the wave periods occur in the range 8—10 s. In general, wave periods for this scenario will increase by end-of-the-century, where 18.3% of the wave periods with 8—10 s are in the range between 0.5—1 m in height.

4.3. Climate change and extreme values of mean significant wave heights

To evaluate the Chabahar coastal vulnerability, it is necessary to calculate mean significant wave heights with 25, 50, and 100-year return periods. Additionally, one of the most important parameters in determining vulnerable areas with respect to coastal floods is significant wave heights. Thus, once climate change impacts were modeled for the time 2071—2100 (30 years) under A1B and A2 scenarios, statistical computations were completed to estimate wave heights for the 25, 50, and 100-year return periods and at-risk coastal areas were determined based on statistical analysis. Fig. 20 shows wave heights under the two A1B and A2 climate change scenarios for the three 25, 50, and 100-year return periods. For these calculations, three distribution functions were considered, namely log-normal, Weibull, and Gumbel. Finally, based on an evaluation of chi-squared test, the Weibull distribution function was selected.

According to Fig. 20 and under the A1B scenario, the mean significant wave heights for 25, 50, and 100-year return periods were 6.1, 6.7, and 7.6 m, respectively; and for the A2 scenario, the mean significant wave heights for 25, 50, and 100-year return periods were calculated as 8.4, 11.0, and 13.7 m, respectively. The results show that the mean significant wave heights under the A2 scenario is considerably higher than those under the A1B scenario; and according to these estimates, the areas influenced by such waves are also augmenting.

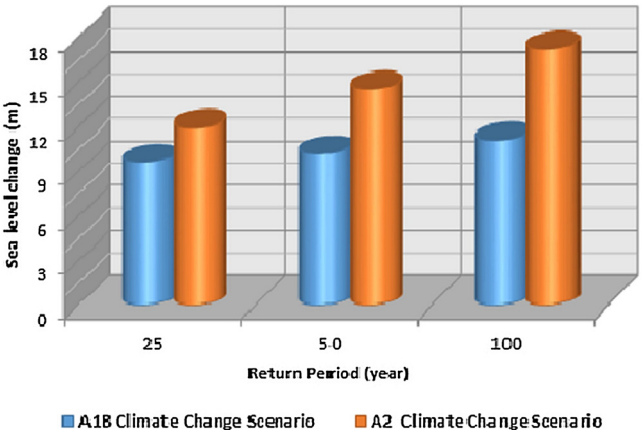

Figure 21 Sea level changes for A1B and A2 climate change scenarios for the three 25, 50, and 100-year return periods.

4.4. Extreme values of sea levels for climate change scenarios

The purpose of the present study is to investigate the coastal vulnerability in Chabahar Bay; thus, the maximum sea levels under both scenarios were calculated. In order to calculate maximum sea levels, three parameters are considered, including global mean sea level, maximum tidal wave height, and significant wave heights. Thus, we assess vulnerability for this region based on possibly severe climate change scenarios to 2100.

According to Fig. 21, the results indicate that under A1B scenario, the sea level change with 25, 50, and 100-year return periods will increase by 9.7, 10.3, and 11.2 m, respectively, and for A2 scenario, will increase by 11.9, 14.6, and 17.3 m for 25, 50, and 100-year return periods, respectively.

4.5. Zoning of water level in Chabahar

In the study area, after determining wave heights for the 25, 50, and 100-year return periods, inundation should be estimated. A flood inundation map was created in order to estimate vulnerable areas, as shown in Fig. 22, taking into account significant wave heights, mean sea level rise, and tidal heights. Clearly, the potential impact might be large,

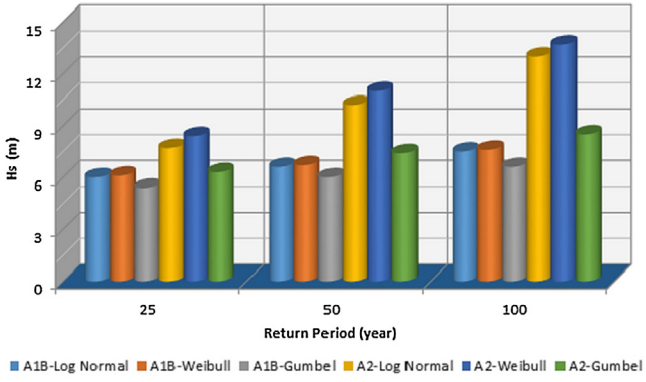

Figure 20 Mean significant wave heights for A1B and A2 climate change scenarios for the three 25, 50, and 100-year return periods.

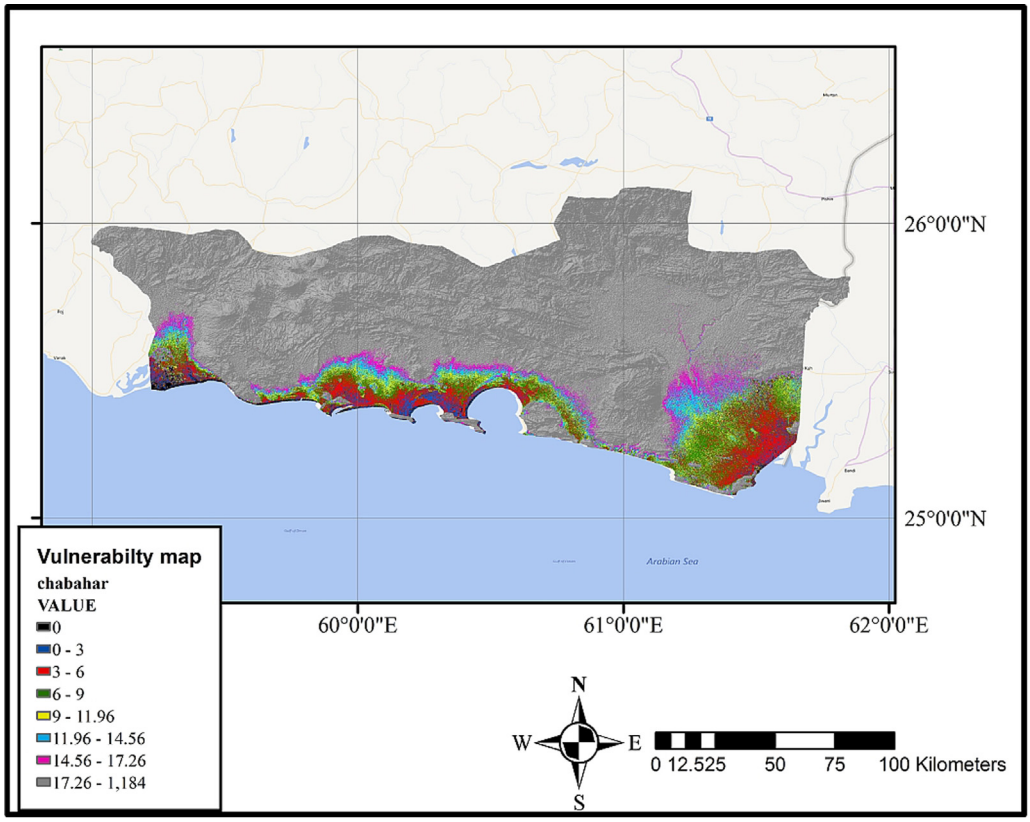

Figure 22 Potential inundation map for end-of-the-century taking into account possible climate change impacts on significant wave heights, mean sea level rise, and tidal heights.

implying that mitigation measures may need to be implemented.

5. Conclusions

To have sustainable development in coastal areas, attention should be drawn to present climate conditions as well as possible future climate scenarios. The present study focuses on the possible effects of climate changes on wind-wave characteristics in Chabahar Bay. In this regard, using wind data as well as bathymetric data of the study area, the wind-wave model was implemented as part of the MIKE21 model system. Next, the model outputs were compared and calibrated with data from buoy located in Chabahar Bay, using statistical methods. Once a model performance was shown reliable, it was run for an 11-year calibration period. Then, using the flow model of MIKE21, the sea level was simulated.

To predict the effect of climate change, global climate model data (CGCM3.1) was downscaled for A1B and A2 scenarios. Results suggest that in comparison to the current climate regimes, there is a notable potential for coastal inundation in the future climate, 2071—2100, and increased Hs wave climate, particularly in regard to the A2 climatic change scenario. Clearly, additional studies are needed, including ensembles of simulations, and additional climate scenarios, such as the more recent RCP4.5 and RCP8.5. When a consensus is reached of these additional studies, with some level of reliability, society may need to re-examine policies and protocols guiding offshore and coastal infrastructure and activities, for sure concerns as design criteria and operational procedures, for example in routine situations as well as in emergencies and severe storm events. These considerations might affect a wide range of activities such as offshore and coastal oil and gas developments, marine transport, fisheries, recreational coastal touring, search and rescue, and coastal security.

References

Bindoff, N.L., Willebrand, J., Artale, V., Cazenave, A., Gregory, J., Gulev, S., Hanawa, K., Le Quere, C., Levitus, S., Nojiri, Y., Shum, C.K., Talley, L.D., Unnikrishnan, A.S., 2007. Observations: oceanic climate change and sea level. In: Solomon, S., Qin, D., Manning, M., Chen, Z., Marquis, M., Averyt, K.B., Tignor, M., Miller, H.L. (Eds.), Climate Change 2007: The Physical Science Basis. Contribution of Working Group I to the Fourth Assessment Report of the Intergovernmental Panel on Climate Change. Cambridge Univ. Press, Cambridge, New York, 387—429.

Breslow, P.B., Sailor, D.J., 2002. Vulnerability of wind power resources to climate change in the continental United States. Renew. Energ. 27 (4), 585—598, http://dx.doi.org/10.1016/S0960-1481(01)00110-0.

Chini, N., Stansby, P., Leake, J., Wolf, J., Roberts-Jones, J., Lowe, J., 2010. The impact of sea level rise and climate change on inshore wave climate: A case study for East Anglia (UK). Coast. Eng. 57 (11—12), 973—984, http://dx.doi.org/10.1016/j.coastaleng.2010.05.009.

Dastgheib, A., Reyns, J., Thammasittirong, S., Weesakul, S., Thatcher, M., Ranasinghe, R., 2016. Variations in the wave climate and sediment transport due to climate change along the coast of Vietnam. J. Marine Sci. Eng. 4 (4), 86, http://dx.doi.org/10.3390/jmse4040086.

DHI, 2005. Mike21 spectral wave module. Sci. Document. Danish Hydraulic Institute (DHI).

Duan, W., He, B., Takara, K., Luo, P., Hu, M., Alias, N.E., Ishihara, M., Wang, Y., 2014. Climate change impacts on wave characteristics along the coast of Japan from 1986 to 2012. J. Coast. Res. 86 (Special Issue 1), 97—104, http://dx.doi.org/10.2112/SI68-013.1.

Goharnejad, H., Shamsai, A., Hosseini, S.A., 2013. Vulnerability assessment of southern coastal areas of Iran to sea level rise: evaluation of climate change impact. Oceanologia 55 (3), 611—637, http://dx.doi.org/10.5697/oc.55-3.611.

Guo, L., Perrie, W., Long, Z., Toulany, B., Sheng, J., 2015. The impacts of climate change on the North Atlantic wave climate. Atmos. Ocean 53 (5), 1—19, http://dx.doi.org/10.1080/07055900.2015.1103697.

Gutmann, E.D., Rasmussen, R.M., Liu, C., Ikeda, K., Gochis, D.J., Clark, M.P., Dudhia, J., Thompson, G., 2012. A comparison of statistical and dynamical downscaling of winter precipitation over complex terrain. J. Climate 25, 262—281, http://dx.doi.org/10.1175/2011JCLI4109.1.

Horton, R., Herweijer, C., Rosenzweig, C., Liu, J., Gornitz, V., Ruane, A.C., 2008. Sea level rise projections for current generation CGCMs based on the semiempirical method. Geophys. Res. Lett. 35 (2), L02715, http://dx.doi.org/10.1029/2007GL032486.

Houghton, J.T., Ding, Y., Griggs, D.J., Noguer, M., van der Linden, P.J., Xiaosu, D. (Eds.), 2001. Climate Change 2001: The Scientific Basis. Contribution of Working Group I to the Third Assessment Report of the Intergovernmental Panel on Climate Change. Cambridge Univ. Press, Cambridge, New York, 639—693.

Intergovernmental Panel on Climate Change (IPCC), 2001. In: Houghton, J.T., Ding, Y., Griggs, D.J., Noguer, M., van der Linden, P.J., Dai, X., Maskell, K., Johnson, C.A. (Eds.), Climate Change 2001: The Scientific Basis. Contribution of Working Group I to the Third Assessment Report of the Intergovernmental Panel on Climate Change. Cambridge Univ. Press, Cambridge, New York, 881 pp.

Intergovernmental Panel on Climate Change (IPCC), 2007. In: Solomon, S., Qin, D., Manning, M., Chen, Z., Marquis, M., Averyt, K.B., Tignor, M., Miller, H.L. (Eds.), Climate Change 2007: The Physical Science Basis. Contribution of Working Group I to the Fourth Assessment Report of the Intergovernmental Panel on Climate Change. Cambridge Univ. Press, Cambridge, New York, 996 pp.

Jevrejeva, S., Moore, J.C., Grinsted, A., 2010. How will sea level respond to changes in natural and anthropogenic forcings by 2100? Geophys. Res. Lett. 37 (7), L07703, http://dx.doi.org/10.1029/2010GL042947.

Kamranzad, B., 2014. Assessment of the changes in average wind speed in Chabahar, Gulf of Oman, due to climate change. Int. J. Maritime Tech. 19, 13—20, (in Persian).

Kamranzad, B., Etemad-Shahidi, A., Chegini, V., Hadadpour, S., 2013. Assessment of CGCM 3.1 wind field in the Persian Gulf. J. Coast. Res. 65, 249—253, http://dx.doi.org/10.2112/SI65-043.1.

Karymbalis, E., Chalkias, C., Chalkias, G., Grigoropoulou, E., Manthos, G., Ferentinou, M., 2012. Assessment of the sensitivity of the southern coast of the Gulf of Corinth (Peloponnese, Greece) to sea-level rise. Cent. Eur. J. Geosci. 4 (4), 561—577.

Mitchell, J.A., Bett, P.E., Hanlon, H.M., Saulter, A., 2015. Investigating the impact of climate change on the UK wave power climate. Meteorol. Z. 26 (3), 291—306, http://dx.doi.org/10.1127/metz/2016/0757.

Pantusa, D., D'Alessandro, F., Riefolo, L., Principato, F., Tomasicchio, G., 2018. Application of a Coastal Vulnerability Index. A case study along the Apulian coastline, Italy. Water 10 (9), 1218, http://dx.doi.org/10.3390/w10091218.

Pendleton, E.A., Thieler, E.R., Williams, S.J., 2005. Coastal vulnerability assessment of Cape Hatteras National Seashore (CAHA) to sea-level rise. Open-file Rep., http://dx.doi.org/10.3133/ofr20041064 20 pp.

Pfeffer, W.T., Harper, J.T., O'Neel, S., 2008. Kinematic constraints on glacier contributions to 21st-century sea-level rise. Science 321 (5894), 1340—1343, http://dx.doi.org/10.1126/science.1159099.

Rahimipouri, H., Gharibreza, M., Isaee, H., Dolatshahi, M., 2006. Hydrodynamic of Currents and Prediction of Erosion and Sedimentation Pattern of the GB. Soil Conservation and Watershed Management Res. Inst., Tehran, 246 pp.

Rahmstorf, 2007. A semi-empirical approach to projecting future sea level rise. Science 315 (5810), 368—370, http://dx.doi.org/10.1126/science.1135456.

Shirinmanesh, S., Chegini, V., 2014. Tidal energy extraction in Chabahar Bay. Geosciences 24 (93) (in Persian).

Stone, M.C., Hotchkiss, R.H., Mearns, L.O., 2003. Water yield responses to high and low spatial resolution climate change scenarios in the Missouri River Basin. Geophys. Res. Lett. 30 (4), 1186, http://dx.doi.org/10.1029/2002GL016122.

Tragaki, A., Gallousi, C., Karymbalis, E., 2018. Coastal hazard vulnerability assessment based on geomorphic, oceanographic and demographic parameters: the case of the Peloponnese (Southern Greece). Land 7 (2), 56, http://dx.doi.org/10.3390/land7020056.

Trzaska, S., Schnarr, E., 2014. A review of downscaling methods for climate change projections. US Agency Internat. Develop., Tetra Tech ARD, 1—42.

Vanem, E., Natvig, B., Huseby, A.B., 2012. Modelling the effect of climate change on the wave climate of the world's oceans. Ocean Sci. J. 47 (2), 123—145, http://dx.doi.org/10.1007/s12601-012-0013-7.

Wandres, M., Pattiaratchi, C., 2017. Projected changes of the southwest Australian wave climate under two atmospheric greenhouse gas concentration pathways. Ocean Model. 117, 70—87.

WCRP Global Sea Level Budget Group, 2018. Global sea-level budget 1993—present. Earth System Sci. Data 10, 1551—1590, http://dx.doi.org/10.5194/essd-10-1551-2018.

Wojtysiak, K., Herman, A., Moskalik, M., 2018. Wind wave climate of west Spitsbergen: seasonal variability and extreme events. Oceanologia 60 (3), 331—343, http://dx.doi.org/10.1016/j.oceano.2018.01.002.